Journal of Power Sources 217 (2012) 209–219

Contents lists available at SciVerse ScienceDirect

Journal of Power Sources

journal homepage: www.elsevier.com/locate/jpowsour

Robustness analysis of State-of-Charge estimation methods for two types of Li-ion batteries

Xiaosong Hu [a,b,*], Shengbo Li [a,c], Huei Peng [a], Fengchun Sun [b]

[a] Department of Mechanical Engineering, The University of Michigan, Ann Arbor, MI 48109, USA
[b] National Engineering Laboratory for Electric Vehicles, Beijing Institute of Technology, No. 5 South Zhongguancun Street, Haidian District, Beijing 100081, China
[c] State Key Laboratory of Automotive Safety and Energy, Tsinghua University, Beijing 100084, China

HIGHLIGHTS

- Analytic functions describing the battery model parameters are optimized.
- EKF based on the optimal analytic model is adopted as the SOC estimator.
- The robustness of the SOC estimator against varying loading profiles is evaluated.
- The robustness of the SOC estimator against varying temperatures is analyzed.
- The robustness of the SOC estimator against varying aging levels is assessed.

ARTICLE INFO

Article history:
Received 18 April 2012
Received in revised form
29 May 2012
Accepted 1 June 2012
Available online 9 June 2012

Keywords:
Battery management systems
SOC estimation
Li-ion battery
Robustness analysis

ABSTRACT

Battery State of Charge (SOC) estimation is an important function for battery management systems and critical for the reliable operations of batteries. This paper analyzes the robustness of SOC estimation algorithms for two types of Li-ion batteries under varying loading conditions, temperatures and aging levels. Based on the model templates identified in an earlier research, the model parameters are determined. The Extended Kalman Filter (EKF) technique is then adopted as the SOC estimation algorithm. The robustness of the estimator against varying loading profiles and temperatures is evaluated and compared against the Coulomb counting method. We subsequently used data from cells that have significantly aged to assess the robustness of the SOC estimation algorithm. Finally, the need for model parameter updates is analyzed.

1. Introduction

Electrified vehicles including battery electric vehicles (BEVs), hybrid electric vehicles (HEVs) and plug-in hybrid electric vehicles (PHEVs) have been actively studied and developed. A critical element for their successful commercialization is technologies for reliable battery operations. Battery management systems (BMS) have been designed to provide monitoring, diagnosis, and control functions to enhance the operations of battery packs. A key function of BMS is to accurately estimate battery state of charge (SOC). Poor SOC estimation can result in larger SOC swing than specified, and can lead to reduced cycle life or lower efficiency.

The Coulomb counting method was often used as a core technology for battery SOC estimation [1–3]. This method is easy to implement but has three challenges. First, the initial SOC at key-on must be estimated accurately because subsequent estimates may be biased by the initial SOC error [4]. Secondly, the method is highly dependent on the accuracy of the current sensor. The current sensor is often subject to noise, drift induced by temperature and other uncertainties. Finally, the battery capacity reduces with age and will affect SOC calculation. To remedy these three challenges, periodic resets are needed. In actual vehicle operations, the open circuit voltage (OCV) is often used to calculate initial SOC. Since there is typically a monotonic relationship between OCV and SOC. Inverting this algebraic relation leads to a SOC estimate. However, error can exist if the battery is not fully relaxed. Sometimes the OCV–SOC curve is very flat in the middle region (e.g., between 30 and 80% SOC), particularly for lithium iron phosphate cells. A small OCV error can result in a large SOC error. Hence, the OCV-based

* Corresponding author. National Engineering Laboratory for Electric Vehicles, Beijing Institute of Technology, No. 5 South Zhongguancun Street, Haidian District, Beijing 100081, China. Tel./fax: +86 10 6891 4625.
E-mail addresses: huxstank@bit.edu.cn, huxiaos@umich.edu (X. Hu).

0378-7753/$ – see front matter © 2012 Elsevier B.V. All rights reserved.
http://dx.doi.org/10.1016/j.jpowsour.2012.06.005

Table 1
Equations of the best performing models identified in Ref. [24].

Model	Equations
(1) First-order RC model for LiNMC cell	$U_{k+1} = \exp(-\Delta t/\tau_1)U_k + R_1[1-\exp(-\Delta t/\tau_1)]I_k$ $V_k = V_{oc}(z_k) - R_0 I_k - U_k$ where I, V and z are current, output voltage and SOC, respectively. Δt is the sampling time and V_{oc} is OCV. R_0 is the internal ohmic resistance which depends on the current direction. U and $\tau_1 = R_1C_1$ are the voltage and time constant of the RC network.
(2) First-order RC model with one-state hysteresis for $LiFePO_4$ cell	$\begin{cases} U_{k+1} = \exp(-\Delta t/\tau_1)U_k + R_1[1-\exp(-\Delta t/\tau_1)]I_k \\ h_{k+1} = \exp(-\lvert\kappa I_k \Delta t\rvert)h_k + [1-\exp(-\lvert\kappa I_k \Delta t\rvert)]H \end{cases}$ $V_k = V_{oc}(z_k) - R_0 I_k - U_k + h_k$ where h is the hysteresis voltage, κ is a decaying factor and H is the maximum amount of hysteresis voltage which is positive for charge and negative for discharge.

reset is not suitable for batteries that are mostly half-charged. For EVs/PHEVs, the reset can be more effectively done, since the SOC frequently reach the two ends where the OCV–SOC slope is steep.

Many SOC estimation models have been proposed, such as artificial neural networks based models [5–7], fuzzy logic models [8,9] and support vector regression (SVR) based models [10,11]. The robustness of these models strongly relies on the quantity and quality of the training data set. A limited training data set (e.g., obtained from new cells) may result in limited model robustness, thus reducing the applicability of the model.

Kalman filter and other observer-based approaches have also been used to estimate the battery SOC. These methods use output feedback and can have better robustness than non-feedback methods. In Refs. [12–14], an Extended Kalman filter (EKF), based on several nonlinear state-space models, was used to estimate the SOC of an HEV Li-polymer cell. A central difference Kalman filter (CDKF) using a nonlinear enhanced self-correcting battery model was also developed to estimate SOC [15,16]. An unscented Kalman filter (UKF) by means of a nonlinear electrochemical battery model was also used to estimate SOC of a lithium-ion cell [17]. The performance of these filters depends on the model accuracy. The sigma-point based CDKF/UKF often provides better estimates than EKF at the expense of higher complexity and computational cost. Several variants of Kalman filter were also studied with similar results [18–20]. Besides Kalman filters, sliding-mode observers [21,22] and linear parameter-varying observers [23] were also applied to predict the battery SOC.

Most of the estimation methods described above were validated using battery data under a narrow set of scenarios, without exploring different temperatures, battery ages, or highly transient loadings. In other words, the robustness of these SOC estimation algorithms was not sufficiently assessed. For example, many SOC estimation approaches mentioned above were evaluated under only one battery loading profile and one environmental temperature. Moreover, the performance and robustness of these SOC algorithms against aging were not adequately studied. A key contribution of this paper is that the SOC estimator performance for two types of Li-ion batteries was evaluated under different loading profiles, temperatures, and cell aging levels.

Table 2
Candidate OCV functions evaluated in this paper.

No.	OCV functions and description
(1)	$V_{oc} = K_0 - K_1/z - K_2 z + K_3 \ln(z) + K_4 \ln(1-z)$ [13] where V_{oc} and z are the OCV and SOC, respectively. The optimization variable vector $\boldsymbol{\theta} = [K_0, K_1, K_2, K_3, K_4]$.
(2)	$V_{oc} = K_0 + \alpha_1 z + \alpha_2(1-e^{-\alpha_3 z}) + \alpha_4(1-e^{-\alpha_5/1-z})$ [26] where $\boldsymbol{\theta} = [K_0, \alpha_1, \alpha_2, \alpha_3, \alpha_4, \alpha_5]$.
(3)	$V_{oc} = K_0 - \alpha_1/z + \alpha_2 e^{-\alpha_3(1-z)}$ [27] where $\boldsymbol{\theta} = [K_0, \alpha_1, \alpha_2, \alpha_3]$.
(4)	$V_{oc} = \alpha_1 e^{-\alpha_2 z} + \alpha_3 + \alpha_4 z + \alpha_5 z^2 + \alpha_6 z^3$ [28] where $\boldsymbol{\theta} = [\alpha_1, \alpha_2, \alpha_3, \alpha_4, \alpha_5, \alpha_6]$.
(5)	$V_{oc} = \alpha_1 z^6 + \alpha_2 z^5 + \alpha_3 z^4 + \alpha_4 z^3 + \alpha_5 z^2 + \alpha_6 z + \alpha_7$ [29] where $\boldsymbol{\theta} = [\alpha_1, \alpha_2, \alpha_3, \alpha_4, \alpha_5, \alpha_6, \alpha_7]$.

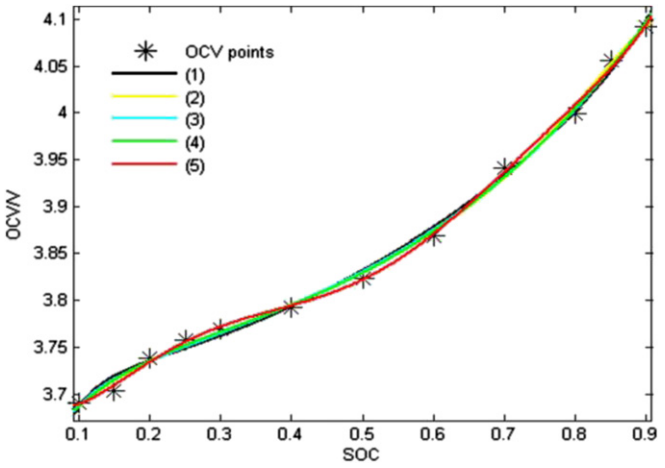

Fig. 2. OCV fitting results for LiNMC cell at 22 °C.

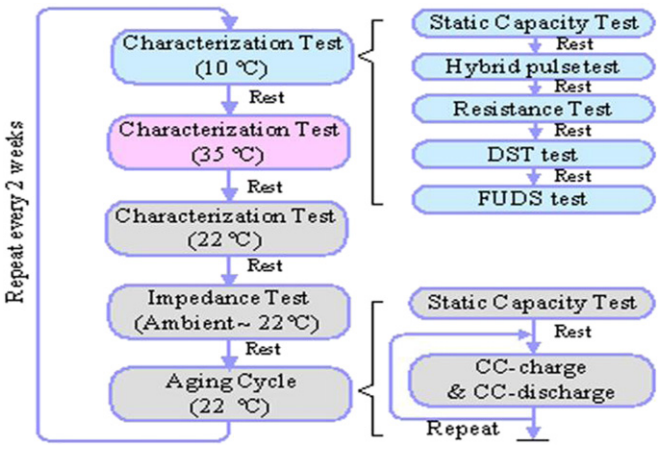

Fig. 1. The test schedule to collect battery cell data.

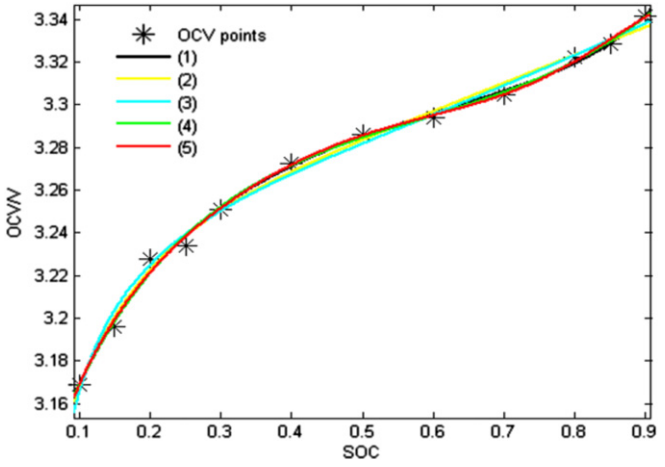

Fig. 3. OCV fitting results for $LiFePO_4$ cell at 22 °C.

Table 3
Three candidate analytic functions for RC and hysteresis parameters.

Type	Functions and description
(1) Polynomial [29]	$f = c_n z^n + c_{n-1} z^{n-1} + \cdots + c_0$ where f and z are model parameter and SOC, respectively. n is the degree of the polynomial. c_n is a coefficient to be optimized.
(2) Exponential [28]	$f = c_1 e^{-c_2 z} + c_3$
(3) Power series [30]	$f = c_1 z^{c_2} + c_3$

Based on the preferred model structures identified in our earlier work [24], the optimal analytic functions explicitly depicting the dependency of model parameters on SOC and temperature are determined. These models are then used in EKF to estimate SOC. The robustness of the estimator under varying loading profiles, temperatures and cell age are then analyzed.

The remainder of this paper is organized as follows. In Section 2, determination of the optimal analytic functions to explicitly delineate the model dependence on SOC and temperature is described. In Section 3, the EKF-based SOC estimator is introduced. The evaluation results of the estimator robustness are discussed in Section 4, followed by conclusions in Section 5.

2. Optimization of model dependency on SOC and temperature

In Ref. [24], we studied twelve equivalent circuit battery model structures reported in the literature, and compared their complexity, training and validation accuracies using test data from multiple cells. The preferred model structures for the lithium nickel–manganese–cobalt oxide (LiNMC) UR14650P and lithium iron phosphate ($LiFePO_4$) APR18650M1A cells were found to be the first-order resistance–capacitance (RC) model and the first-order RC model with one-state hysteresis, respectively. The equations of the two models are shown in Table 1. The aim of Ref. [24] was to find the optimal model structures and the parameters of all the twelve models were assumed to be constant (independent of SOC). To explore the full potential of these two preferred model structures, in this paper we will establish the dependence of model parameters on the battery SOC and temperature. The test schedules shown in Fig. 1 are designed to excite and age the two types of battery cells. The datasets are described in details in Ref. [24]. The three dynamic test cycles (Hybrid Pulse Test DST and FUDS) are used to identify the SOC and temperature-dependent analytic functions.

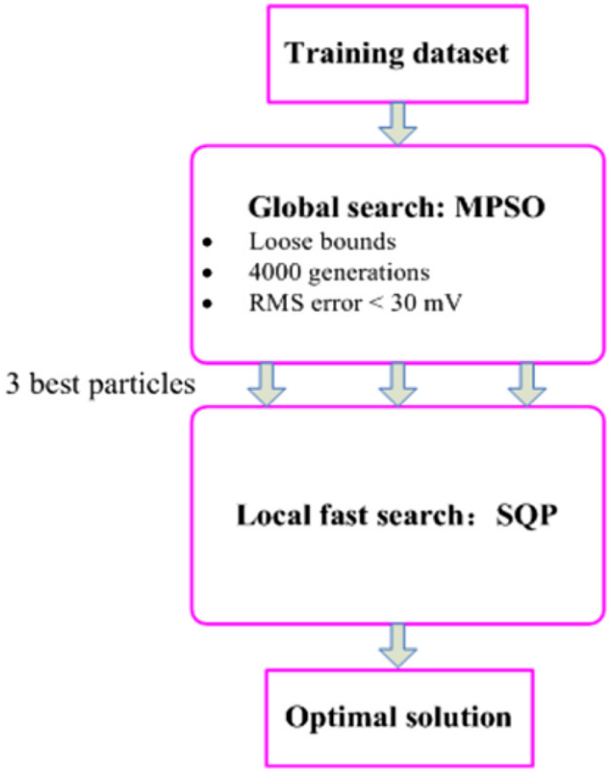

Fig. 4. Schematic diagram of the two-step optimization process.

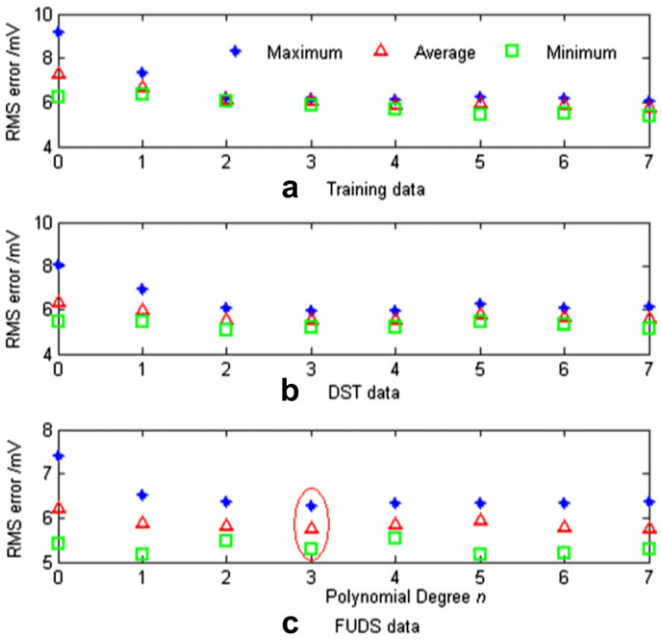

Fig. 5. Comparison results of polynomials with different degrees for the LiNMC cell.

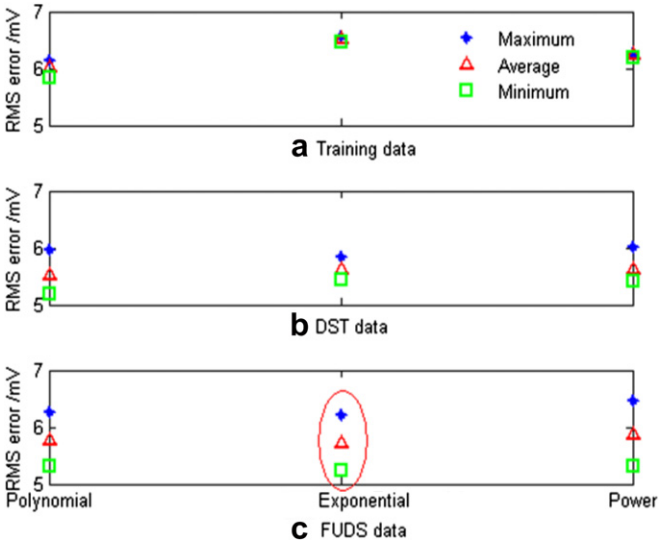

Fig. 6. Comparison results of the three types of analytic functions for the LiNMC cell.

Table 4
Optimal coefficients of the analytic functions for the LiNMC cell.

Parameter	Coefficients
OCV	$V_{oc} = \alpha_1 z^6 + \alpha_2 z^5 + \alpha_3 z^4 + \alpha_4 z^3 + \alpha_5 z^2 + \alpha_6 z + \alpha_7$ $(0.1 \le z \le 0.9)$
	where
	$\alpha_1 = \{-0.1674(\mathrm{Te}-10)+2.9192,\ 10 \le \mathrm{Te} < 22\ (\mathrm{Te}:\mathrm{Temperature});\ 0.1939(\mathrm{Te}-22)+0.9109,\ 22 \le \mathrm{Te} \le 35\}$
	$\alpha_2 = \{0.3394(\mathrm{Te}-10)-5.8608,\ 10 \le \mathrm{Te} < 22;\ -0.3675(\mathrm{Te}-22)-1.7875,\ 22 \le \mathrm{Te} \le 35\}$
	$\alpha_3 = \{-0.1811(\mathrm{Te}-10)+1.3408,\ 10 \le \mathrm{Te} < 22;\ 0.0469(\mathrm{Te}-22)-0.8330,\ 22 \le \mathrm{Te} \le 35\}$
	$\alpha_4 = \{-0.0614(\mathrm{Te}-10)+5.1684,\ 10 \le \mathrm{Te} < 22;\ 0.3023(\mathrm{Te}-22)+4.4320,\ 22 \le \mathrm{Te} \le 35\}$
	$\alpha_5 = \{0.0948(\mathrm{Te}-10)-4.4983,\ 10 \le \mathrm{Te} < 22;\ -0.2336(\mathrm{Te}-22)-3.3606,\ 22 \le \mathrm{Te} \le 35\}$
	$\alpha_6 = \{-0.0290(\mathrm{Te}-10)+1.5815, 10 \le \mathrm{Te} < 22;\ 0.0648(\mathrm{Te}-22)+1.2331,\ 22 \le \mathrm{Te} \le 35\}$
	$\alpha_7 = \{0.0025(\mathrm{Te}-10)+3.5600,\ 10 \le \mathrm{Te} < 22;\ -0.0063(\mathrm{Te}-22)+3.5901,\ 22 \le \mathrm{Te} \le 35\}$
Charging R_0^-	$R_0^- = c_1 e^{-c_2 z} + c_3$ $(0.1 \le z \le 0.9)$
	where
	$c_1 = \{-0.0116(\mathrm{Te}-10)+0.1728,\ 10 \le \mathrm{Te} < 22;\ 0.0741(\mathrm{Te}-22)+0.0337,\ 22 \le \mathrm{Te} \le 35\}$
	$c_2 = \{0.5632(\mathrm{Te}-10)-24.5426,\ 10 \le \mathrm{Te} < 22;\ -1.0925(\mathrm{Te}-22)-17.7848,\ 22 \le \mathrm{Te} \le 35\}$
	$c_3 = \{-0.0009(\mathrm{Te}-10)+0.1086, 10 \le \mathrm{Te} < 22;\ -0.0005(\mathrm{Te}-22)+0.0972,\ 22 \le \mathrm{Te} \le 35\}$
Discharging R_0^+	$R_0^+ = c_1 e^{-c_2 z} + c_3$ $(0.1 \le z \le 0.9)$
	where
	$c_1 = \{0.0072(\mathrm{Te}-10)+0.0761,\ 10 \le \mathrm{Te} < 22;\ -0.0125(\mathrm{Te}-22)+0.1621,\ 22 \le \mathrm{Te} \le 35\}$
	$c_2 = \{-2.0975(\mathrm{Te}-10)-4.7917,\ 10 \le \mathrm{Te} < 22;\ -0.6137(\mathrm{Te}-22)-29.9621,\ 22 \le \mathrm{Te} \le 35\}$
	$c_3 = \{-0.0010(\mathrm{Te}-10)+0.1142,\ 10 \le \mathrm{Te} < 22;\ -0.0006(\mathrm{Te}-22)+0.1021,\ 22 \le \mathrm{Te} \le 35\}$
R_1 (RC network)	$R_1 = c_1 e^{-c_2 z} + c_3$ $(0.1 \le z \le 0.9)$
	where
	$c_1 = \{0,\ 10 \le \mathrm{Te} < 22;\ 0,\ 22 \le \mathrm{Te} \le 35\}$ $c_2 = \{-0.1403(\mathrm{Te}-10)-21.9590,\ 10 \le \mathrm{Te} < 22;\ -0.6098(\mathrm{Te}-22)-23.6430,\ 22 \le \mathrm{Te} \le 35\}$
	$c_3 = \{-0.0015(\mathrm{Te}-10)+0.0608,\ 10 \le \mathrm{Te} < 22;\ -0.0011(\mathrm{Te}-22)+0.0433,\ 22 \le \mathrm{Te} \le 35\}$
Time constant τ_1 (RC network)	$\tau_1 = c_1 e^{-c_2 z} + c_3$ $(0.1 \le z \le 0.9)$
	where
	$c_1 = \{2.1871(\mathrm{Te}-10)+19.3967,\ 10 \le \mathrm{Te} < 22;\ -1.9460(\mathrm{Te}-22)+45.6424,\ 22 \le \mathrm{Te} \le 35\}$
	$c_2 = \{-4.1106(\mathrm{Te}-10)-0.6723,\ 10 \le \mathrm{Te} < 22;\ 1.9550(\mathrm{Te}-22)-50.0000,\ 22 \le \mathrm{Te} \le 35\}$
	$c_3 = \{0.5091(\mathrm{Te}-10)+32.7608,\ 10 \le \mathrm{Te} < 22;\ 1.7591(\mathrm{Te}-22)+38.8700,\ 22 \le \mathrm{Te} \le 35\}$

2.1. OCV function identification

Compared to lookup tables, analytic OCV–SOC functions can be beneficial. For example, function derivatives can be calculated more easily and accurately. Several candidate functions proposed in the literature to depict the battery OCV are summarized in Table 2. We fit the five candidate functions shown in Table 2 to the 12 OCV points obtained in [24] by nonlinear least-squares optimization. The results of the LiNMC and $LiFePO_4$ cells at temperature = 22 °C are shown in Figs. 2 and 3, respectively. It seems that all candidate functions work reasonably well and the polynomial (5) matches the OCV points a little better for both cells. The fitting results at temperature = 10 °C and 35 °C are similar. It was argued in Ref. [25] that rich features in low or high SOC can be better fitted by a high-order smooth polynomial. Therefore, function (5) in Table 2 is selected.

2.2. Optimization process for the RC circuit and one-state hysteresis

In Ref. [24], the first-order RC model with one-state hysteresis was found to fit the LiFePO4 cell results the best while the first-order RC model was found to be the best for the LiNMC cells. Three analytic functions commonly used to fit the RC parameters

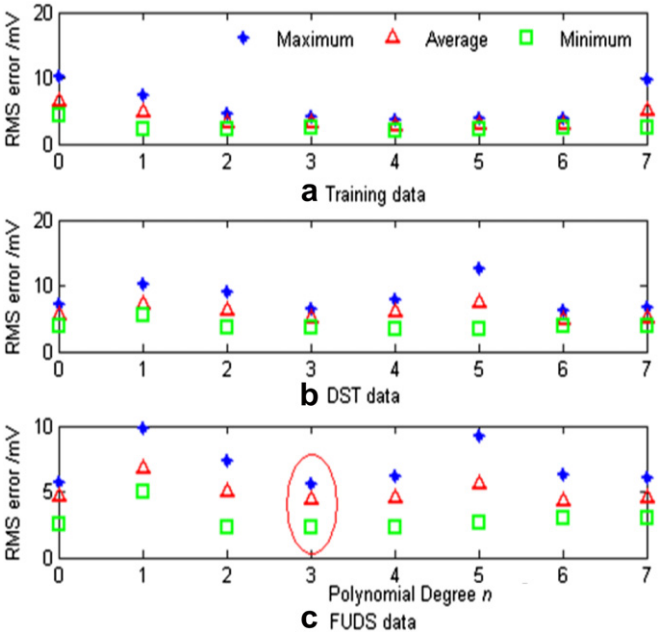

Fig. 7. Comparison results of polynomials with different degrees for the $LiFePO_4$ cell.

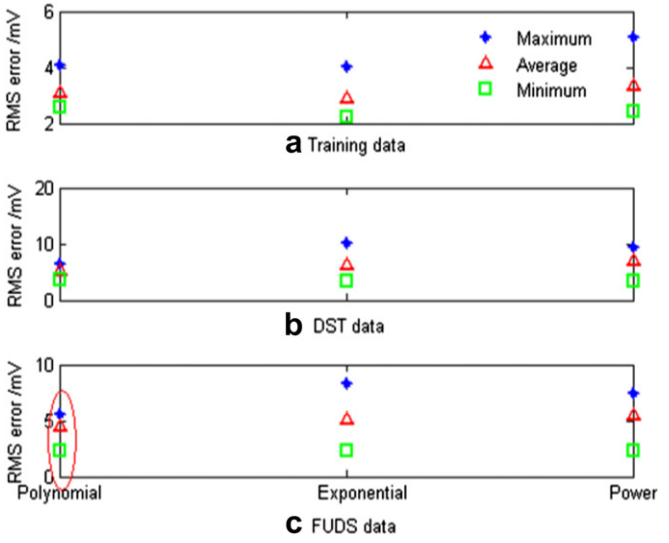

Fig. 8. Comparison results of the three types of analytic functions for the $LiFePO_4$ cell.

are summarized in Table 3. The same basis functions are applied to the hysteresis parameters as well, to reduce the complexity in optimization. Since each model parameter is expressed as an explicit function with unknown coefficients, all are to be found by optimization routines. Furthermore, unlike the model parameters (e.g., internal resistance), we often have no clear knowledge of the bounds of the unknown coefficients. The global multi-swarm particle swarm optimization (MPSO) method [24] is used to optimize these coefficients. However, its computation load is very heavy. If gradient-based methods such as sequential quadratic programming (SQP) are used, they frequently got trapped at local minima. Therefore, a two-step optimization procedure is adopted. The schematic diagram of the two-step optimization is shown in Fig. 4. With loose bounds for all the unknown coefficients, 4000 generations in the global MPSO are first iterated such that the RMS error is less than 30 mV. Then, the 3 best solutions (particles) attained by MPSO are used as the initial solutions of the SQP algorithm. The optimization is conducted under each temperature. Then, we fit piecewise linear functions to the optimal solutions for the three temperatures, thereby establishing an explicit temperature dependency. The OCV coefficients (sixth-degree polynomial) are also optimized in the two-step procedure, together with other model parameters.

(1) LiNMC cell

The results using polynomial basis functions of different degrees are shown in Fig. 5. The maximum, minimum and average RMS errors under three temperatures are computed. The hybrid pulse test dataset is used as the training dataset while the Dynamic Stress Test (DST) and Federal Urban Dynamic Schedule (FUDS) datasets [24] are used as validation datasets. The third-degree polynomial is selected based on accuracy-complexity trade-off. Fig. 6 shows the comparison results of the third-degree polynomial, exponential (2)

Table 5
Optimal coefficients of the analytic functions for the $LiFePO_4$ cell.

Parameter	Coefficients
OCV	$V_{oc} = \alpha_1 z^6 + \alpha_2 z^5 + \alpha_3 z^4 + \alpha_4 z^3 + \alpha_5 z^2 + \alpha_6 z + \alpha_7$ $(0.1 \le z \le 0.9)$ where $\alpha_1 = \{-0.4629(\mathrm{Te}-10)+1.9754,\ 10 \le \mathrm{Te} < 22;\ 0.2506(\mathrm{Te}-22)-3.5795,\ 22 \le \mathrm{Te} \le 35\}$ $a_2 = \{1.0943(\mathrm{Te}-10)-3.6208,\ 10 \le \mathrm{Te} < 22;\ -0.7233(\mathrm{Te}-22)+9.5106,\ 22 \le \mathrm{Te} \le 35\}$ $\alpha_3 = \{-0.8341(\mathrm{Te}-10)+0.0094,\ 10 \le \mathrm{Te} < 22;\ 0.8529(\mathrm{Te}-22)-10.0000,\ 22 \le \mathrm{Te} \le 35\}$ $\alpha_4 = \{0.1023(\mathrm{Te}-10)+4.3001,\ 10 \le \mathrm{Te} < 22;\ -0.4813(\mathrm{Te}-22)+5.5273,\ 22 \le \mathrm{Te} \le 35\}$ $\alpha_5 = \{0.1514(\mathrm{Te}-10)-3.7275,\ 10 \le \mathrm{Te} < 22;\ 0.1121(\mathrm{Te}-22)-1.9108,\ 22 \le \mathrm{Te} \le 35\}$ $\alpha_6 = \{-0.0631(\mathrm{Te}-10)+1.3896,\ 10 \le \mathrm{Te} < 22;\ -0.0049(\mathrm{Te}-22)+0.6326,\ 22 \le \mathrm{Te} \le 35\}$ $\alpha_7 = \{0.0068(\mathrm{Te}-10)+3.0629,\ 10 \le \mathrm{Te} < 22;\ -0.0002(\mathrm{Te}-22)+3.1440,\ 22 \le \mathrm{Te} \le 35\}$
Charging resistance R_0^-	$R_0^- = c_1 z^3 + c_2 z^2 + c_3 z + c_4$ $(0.1 \le z \le 0.9)$ where $c_1 = \{0.0148(\mathrm{Te}-10)-0.1670,\ 10 \le \mathrm{Te} < 22;\ -0.0018(\mathrm{Te}-22)+0.0105,\ 22 \le \mathrm{Te} \le 35\}$ $c_2 = \{-0.0221(\mathrm{Te}-10)+0.2458,\ 10 \le \mathrm{Te} < 22;\ 0.0027(\mathrm{Te}-22)-0.0200,\ 22 \le \mathrm{Te} \le 35\}$ $c_3 = \{0.0098(\mathrm{Te}-10)-0.1027,\ 10 \le \mathrm{Te} < 22;\ -0.0014(\mathrm{Te}-22)+0.0149,\ 22 \le \mathrm{Te} \le 35\}$ $c_4 = \{-0.0016(\mathrm{Te}-10)+0.0349,\ 10 \le \mathrm{Te} < 22;\ -0.0001(\mathrm{Te}-22)+0.0151,\ 22 \le \mathrm{Te} \le 35\}$
Discharging R_0^+	$R_0^+ = c_1 z^3 + c_2 z^2 + c_3 z + c_4$ $(0.1 \le z \le 0.9)$ where $c_1 = \{-0.0012(\mathrm{Te}-10)-0.0010,\ 10 \le \mathrm{Te} < 22;\ 0.0106(\mathrm{Te}-22)-0.0153,\ 22 \le \mathrm{Te} \le 35\}$ $c_2 = \{0.0005(\mathrm{Te}-10)+0.0274,\ 10 \le \mathrm{Te} < 22;\ -0.0163(\mathrm{Te}-22)+0.0333,\ 22 \le \mathrm{Te} \le 35\}$ $c_3 = \{0.0009(\mathrm{Te}-10)-0.0340,\ 10 \le \mathrm{Te} < 22;\ 0.0071(\mathrm{Te}-22)-0.0231,\ 22 \le \mathrm{Te} \le 35\}$ $c_4 = \{-0.0013(\mathrm{Te}-10)+0.0432,\ 10 \le \mathrm{Te} < 22;\ -0.0014(\mathrm{Te}-22)+0.0277,\ 22 \le \mathrm{Te} \le 35\}$
R_1 (RC network)	$\mathrm{R}_1 = c_1 z^3 + c_2 z^2 + c_3 z + c_4$ $(0.1 \le z \le 0.9)$ where $c_1 = \{0.0272(\mathrm{Te}-10)-0.3042,\ 10 \le \mathrm{Te} < 22;\ -0.0058(\mathrm{Te}-22)+0.0220,\ 22 \le \mathrm{Te} \le 35\}$ $c_2 = \{-0.0424(\mathrm{Te}-10)+0.4777,\ 10 \le \mathrm{Te} < 22;\ 0.0078(\mathrm{Te}-22)-0.0309,\ 22 \le \mathrm{Te} \le 35\}$ $c_3 = \{0.0226(\mathrm{Te}-10)-0.2715,\ 10 \le \mathrm{Te} < 22;\ -0.0022(\mathrm{Te}-22)-0.0000,\ 22 \le \mathrm{Te} \le 35\}$ $c_4 = \{-0.0054(\mathrm{Te}-10)+0.0956,\ 10 \le \mathrm{Te} < 22;\ -0.0007(\mathrm{Te}-22)+0.0311,\ 22 \le \mathrm{Te} \le 35\}$
Time constant τ_1 (RC network)	$\tau_1 = c_1 z^3 + c_2 z^2 + c_3 z + c_4$ $(0.1 \le z \le 0.9)$ where $c_1 = \{0.1124(\mathrm{Te}-10)-4.3311,\ 10 \le \mathrm{Te} < 22;\ -0.2546(\mathrm{Te}-22)-2.9824,\ 22 \le \mathrm{Te} \le 35\}$ $c_2 = \{-0.4379(\mathrm{Te}-10)+1.1861,\ 10 \le \mathrm{Te} < 22;\ -0.0584(\mathrm{Te}-22)-4.0682,\ 22 \le \mathrm{Te} \le 35\}$ $c_3 = \{0.2447(\mathrm{Te}-10)+6.2657,\ 10 \le \mathrm{Te} < 22;\ -1.4771(\mathrm{Te}-22)+9.2026,\ 22 \le \mathrm{Te} \le 35\}$ $c_4 = \{-0.9800(\mathrm{Te}-10)+35.2236,\ 10 \le \mathrm{Te} < 22;\ 0.5832(\mathrm{Te}-22)+23.4637,\ 22 \le \mathrm{Te} \le 35\}$
Hysteresis decaying factor κ	$\kappa = c_1 z^3 + c_2 z^2 + c_3 z + c_4$ $(0.1 \le z \le 0.9)$ where $c_1 = \{0.0379(\mathrm{Te}-10)-0.5478,\ 10 \le \mathrm{Te} < 22;\ 0.0243(\mathrm{Te}-22)-0.0925,\ 22 \le \mathrm{Te} \le 35\}$ $c_2 = \{-0.0521(\mathrm{Te}-10)+0.7931,\ 10 \le \mathrm{Te} < 22;\ -0.0339(\mathrm{Te}-22)+0.1675,\ 22 \le \mathrm{Te} \le 35\}$ $c_3 = \{0.0188(\mathrm{Te}-10)-0.3157,\ 10 \le \mathrm{Te} < 22;\ 0.0124(\mathrm{Te}-22)-0.0903,\ 22 \le \mathrm{Te} \le 35\}$ $c_4 = \{-0.0015(\mathrm{Te}-10)+0.0410,\ 10 \le \mathrm{Te} < 22;\ -0.0011(\mathrm{Te}-22)+0.0233,\ 22 \le \mathrm{Te} \le 35\}$
Maximum charging hysteresis H^-	$H^- = c_1 z^3 + c_2 z^2 + c_3 z + c_4$ $(0.1 \le z \le 0.9)$ where $c_1 = \{-0.0248(\mathrm{Te}-10)+0.9525,\ 10 \le \mathrm{Te} < 22;\ -0.0725(\mathrm{Te}-22)+0.6554,\ 22 \le \mathrm{Te} \le 35\}$ $c_2 = \{0.0306(\mathrm{Te}-10)-1.3109,\ 10 \le \mathrm{Te} < 22;\ 0.1021(\mathrm{Te}-22)-0.9440,\ 22 \le \mathrm{Te} \le 35\}$ $c_3 = \{-0.0085(\mathrm{Te}-10)+0.4424,\ 10 \le \mathrm{Te} < 22;\ -0.0331(\mathrm{Te}-22)+0.3399,\ 22 \le \mathrm{Te} \le 35\}$ $c_4 = \{-0.0005(\mathrm{Te}-10)+0.0060,\ 10 \le \mathrm{Te} < 22;\ 0.0018(\mathrm{Te}-22)+0.0000,\ 22 \le \mathrm{Te} \le 35\}$
Maximum discharging hysteresis H^+	$H^+ = c_1 z^3 + c_2 z^2 + c_3 z + c_4$ $(0.1 \le z \le 0.9)$ where $c_1 = \{0.0415(\mathrm{Te}-10)-0.0848,\ 10 \le \mathrm{Te} < 22;\ -0.0091(\mathrm{Te}-22)+0.4134,\ 22 \le \mathrm{Te} \le 35\}$ $c_2 = \{-0.0609(\mathrm{Te}-10)-0.0169,\ 10 \le \mathrm{Te} < 22;\ 0.0165(\mathrm{Te}-22)-0.7478,\ 22 \le \mathrm{Te} \le 35\}$ $c_3 = \{0.0243(\mathrm{Te}-10)+0.0944,\ 10 \le \mathrm{Te} < 22;\ -0.0065(\mathrm{Te}-22)+0.3857,\ 22 \le \mathrm{Te} \le 35\}$ $c_4 = \{-0.0018(\mathrm{Te}-10)-0.0392,\ 10 \le \mathrm{Te} < 22;\ 0.0005(\mathrm{Te}-22)-0.0613,\ 22 \le \mathrm{Te} \le 35\}$

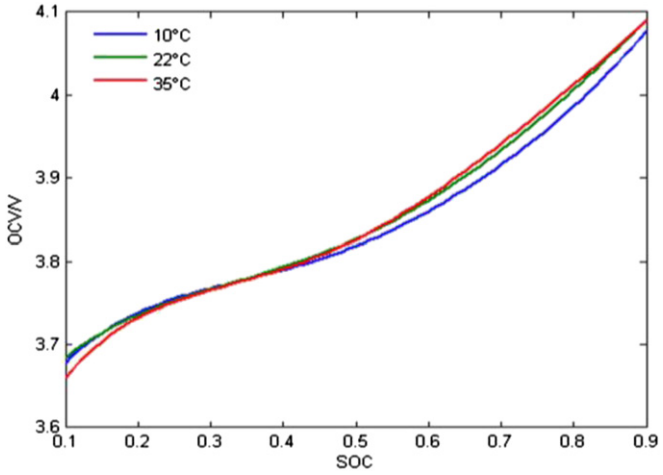

Fig. 9. OCV function of the LiNMC cell.

and power series (3). The results are all very similar (i.e., they all work reasonably well). The exponential function shows slightly better validation accuracy (especially in FUDS data) and is quite simple. Therefore, the exponential function is used to describe the RC parameters of the first-order RC model for the LiNMC cells. The optimal coefficients of the analytic functions are summarized in Table 4.

(2) $LiFePO_4$ cell

Polynomials of different degrees for the $LiFePO_4$ cell are shown in Fig. 7. Fig. 8 shows the performance of the third-degree polynomial, exponential, and power series models. It was found that the third-degree polynomial function shows the best balance between training/validation accuracies and complexity. The optimized coefficients of the analytic functions for the $LiFePO_4$ cell (the first-order RC model with one-state hysteresis) are summarized in Table 5. The OCV functions of the two types of Li-ion batteries are shown in Figs. 9 and 10. It is obvious that the OCV of the $LiFePO_4$ cell between 25% and 85% SOC is much flatter than that of the LiNMC cell. The exact dependence of the model parameters on SOC and temperature are unclear due to the complex reactions and dynamics inside the cells [26]. Furthermore, since we use lumped models to approximate the current–voltage relationships, the model parameters are just estimates with no clear physical

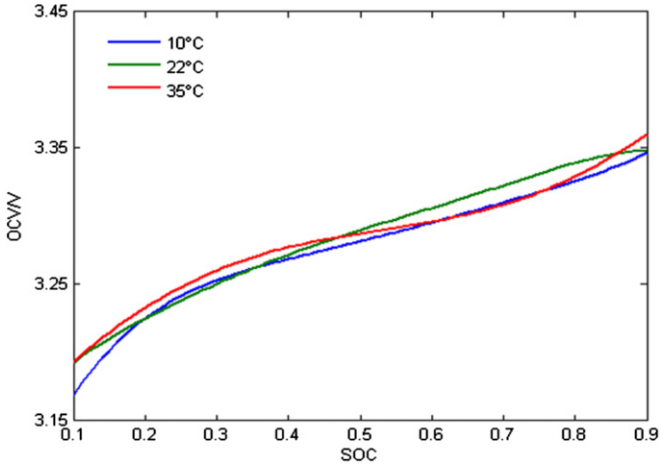

Fig. 10. OCV function of the $LiFePO_4$ cell.

Table 6
EKF equations for the SOC estimation.

Nonlinear battery model

$\boldsymbol{x}_{k+1} = \boldsymbol{A}(z_k, \mathrm{Te})\boldsymbol{x}_k + \boldsymbol{B}(z_k, \mathrm{Te})\boldsymbol{u}_k + \omega_k$

$y_k = g(\boldsymbol{x}_k, I_k) + \nu_k$

where $\boldsymbol{x}$, I and y are state variables, current and voltage, respectively. The first element of $\boldsymbol{x}$ is SOC z. $\boldsymbol{u}$ is the model input. $\boldsymbol{A}$ and $\boldsymbol{B}$ are SOC and temperature-dependent matrices. ω and ν are assumed to be independent, zero-mean, Gaussian noise processes of covariance matrices $\boldsymbol{Q}$ and V.

(1) Initialization

Assign the initial state estimate $\hat{\boldsymbol{x}}_o$, error covariance $\boldsymbol{P}_0$, $\boldsymbol{Q}$ and V.

(2) Prediction

$$\begin{cases} \hat{\boldsymbol{x}}_{k|k-1} = \boldsymbol{A}(\hat{z}_{k-1}, \mathrm{Te})\hat{\boldsymbol{x}}_{k-1} + \boldsymbol{B}\boldsymbol{u}_{k-1} \\ \boldsymbol{P}_{k|k-1} = \boldsymbol{A}(\hat{z}_{k-1}, \mathrm{Te})\boldsymbol{P}_{k-1}\boldsymbol{A}(\hat{z}_{k-1}, \mathrm{Te})^T + \boldsymbol{Q} \end{cases}$$

(3) Correction

$$\begin{cases} \boldsymbol{G}_k = \boldsymbol{P}_{k|k-1}\boldsymbol{C}(\hat{z}_{k|k-1}, \mathrm{Te})^T[\boldsymbol{C}(\hat{z}_{k|k-1}, \mathrm{Te})\boldsymbol{P}_{k|k-1}\boldsymbol{C}(\hat{z}_{k|k-1}, \mathrm{Te})^T + W]^{-1} \\ \hat{\boldsymbol{x}}_k = \hat{\boldsymbol{x}}_{k|k-1} + \boldsymbol{G}_k[y_k - g(\hat{\boldsymbol{x}}_{k|k-1}, I_k)] \\ \boldsymbol{P}_k = [\boldsymbol{E} - \boldsymbol{G}_k\boldsymbol{C}(\hat{z}_k, Te)]\boldsymbol{P}_{k|k-1} \end{cases}$$

where

$$\boldsymbol{C}(\hat{z}_{k|k-1}, Te) = \frac{\partial g(\boldsymbol{x}_k, I_k)}{\partial \boldsymbol{x}_k}\Big|_{\boldsymbol{x}_k = \hat{\boldsymbol{x}}_{k|k-1}}$$

Table 7
Matrices of the state-space models for the LINMC and $LiFePO_4$ cells.

(1) The first-order RC model of the LiNMC cell

$$\boldsymbol{x}_k = \begin{bmatrix} z_k \\ U_k \end{bmatrix}, \boldsymbol{A}(z_k, \mathrm{Te}) = \begin{bmatrix} 1 & 0 \\ 0 & \exp\left(\frac{-\Delta t}{\tau_1}\right) \end{bmatrix}, \boldsymbol{B}(z_k, \mathrm{Te}) = \begin{bmatrix} \frac{-\eta\Delta t}{3600C_n} \\ R_1 - R_1\exp\left(\frac{-\Delta t}{\tau_1}\right) \end{bmatrix},$$

$$g(\boldsymbol{x}_k, I_k) = V_{\mathrm{oc},k} - U_k - I_k^+R_0^+ - I_k^-R_0^-$$

where U is the voltage across the RC network at time k. Δt is the sampling time, η is Coulombic efficiency, and C_n is the cell capacity. I^+ and I^- are discharging and charging currents, respectively. When $I \le 0$ (charging), $I^+ = 0$, $I^- = I$; when $I > 0$ (discharging), $I^- = 0$, $I^+ = I$.

(2) The first-order RC model with hysteresis for the $LiFePO_4$ cell

$$\boldsymbol{x}_k = \begin{matrix} z_k \\ [U_k \\ h_k \end{matrix}], \boldsymbol{A}(z_k, \mathrm{Te}) = \begin{bmatrix} 1 & 0 & 0 \\ 0 & \exp\left(\frac{-\Delta t}{\tau_1}\right) & 0 \\ 0 & 0 & \exp(-|\kappa I_k\Delta t|) \end{bmatrix},$$

$$\boldsymbol{B}(z_k, \mathrm{Te}) = \begin{bmatrix} \frac{-\eta\Delta t}{3600C_n} & 0 \\ R_1 - R_1\exp\left(\frac{-\Delta t}{\tau_1}\right) & 0 \\ 0 & 1 - \exp(-|\kappa I_k\Delta t|) \end{bmatrix},$$

$$\boldsymbol{u} = \left\{ \begin{bmatrix} I \\ H^- \end{bmatrix}, I \le 0;\ \begin{bmatrix} I \\ H^+ \end{bmatrix}, I > 0 \right\}, g(\boldsymbol{x}_k, I_k) = V_{\mathrm{oc},k} - U_k + h_k - I_k^+R_0^+ - I_k^-R_0^-.$$

meanings. Nevertheless, the models were able to represent the lumped behavior of the battery well. With the RMS error around merely 5 mV, the achieved analytic functions can be used to predict battery voltage with adequate accuracy. It should be emphasized, however, that the model error in the validation dataset is much higher. This is perhaps because the hysteresis model was trained

Table 8
Assumed initial SOC error of Coulomb counting for the LiNMC cell.

10 °C	22 °C	35 °C
±3.74%	±3.09%	±3.28%

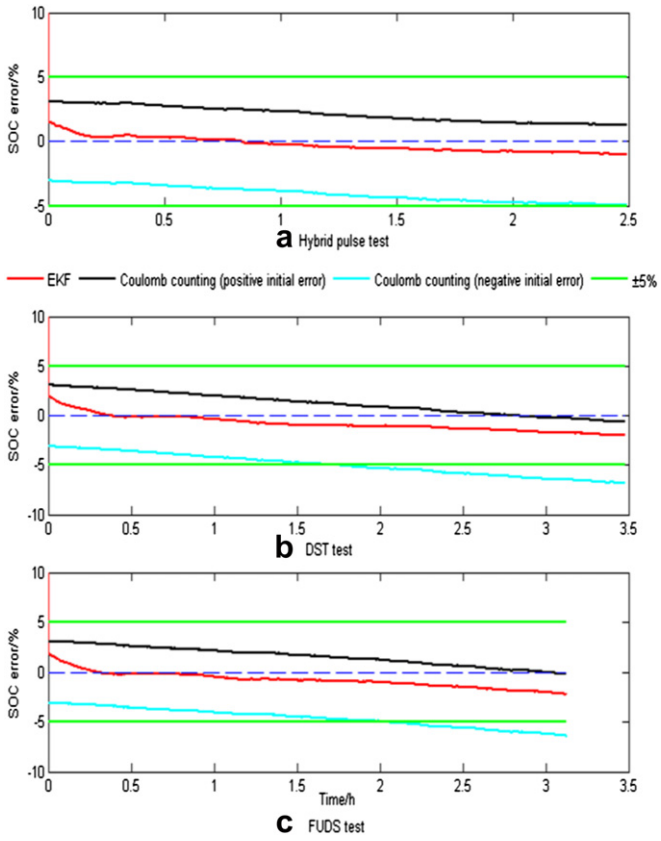

Fig. 11. SOC estimation errors of the LiNMC cell under 22 °C (before aging), (a) hybrid pulse test; (b) DST test; (c) FUDS test.

Table 9
Assumed initial SOC error of Coulomb counting for the $LiFePO_4$ cell.

10 °C	22 °C	35 °C
±6.30%	±5.41%	±9.65%

using less-transient dynamic dataset and during the more significant transient the model error increases.

3. EKF-based SOC estimator

EKF is a widely used state estimation method for nonlinear dynamical systems. Based on the optimal models presented in Section 2, EKF is adopted to estimate the battery SOC. The EKF equations for the SOC estimation are summarized in Table 6. The matrices for the state-space models for the LINMC and $LiFePO_4$ cells are summarized in Table 7.

4. Robustness of the SOC estimator

To better evaluate the robustness of the SOC estimator in an environment close to realistic automotive environment, artificial Gaussian noise is added to the current collected by the Arbin tester. The mean and standard deviation of the noise are −0.01 A and 0.06 A (around 2% of the full range), respectively.

4.1. Robustness against different loading profiles and temperatures

The hybrid pulse test, DST and FUDS datasets collected under three different temperatures for new cells are used in this subsection. The data below 20% SOC is discarded, since the battery SOC is seldom permitted to be less than 20% in actual driving. To better

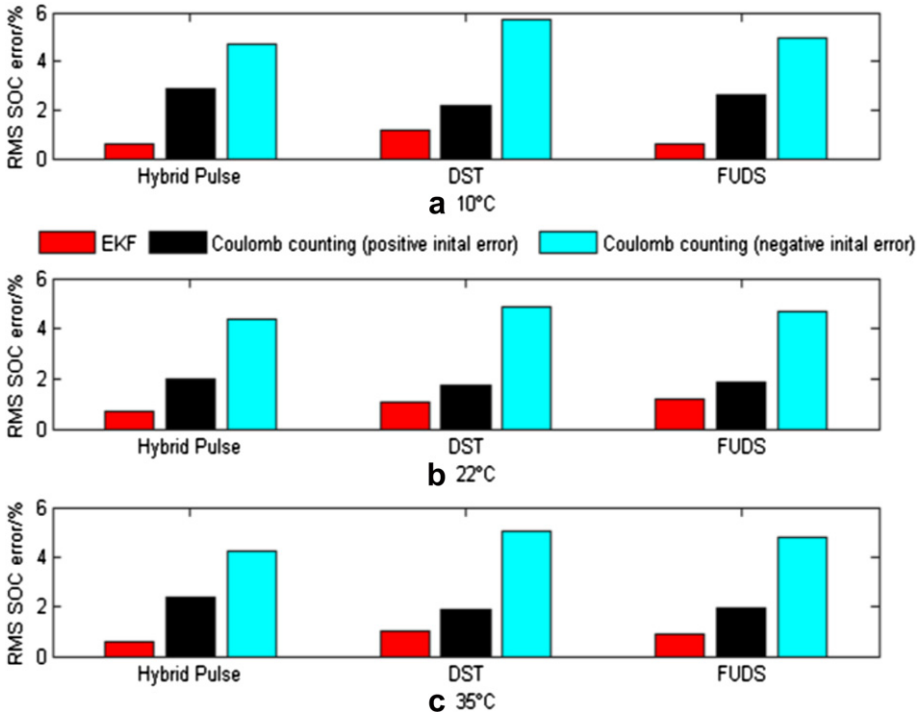

Fig. 12. RMS SOC errors under three temperatures for the LiNMC cell (new cell).

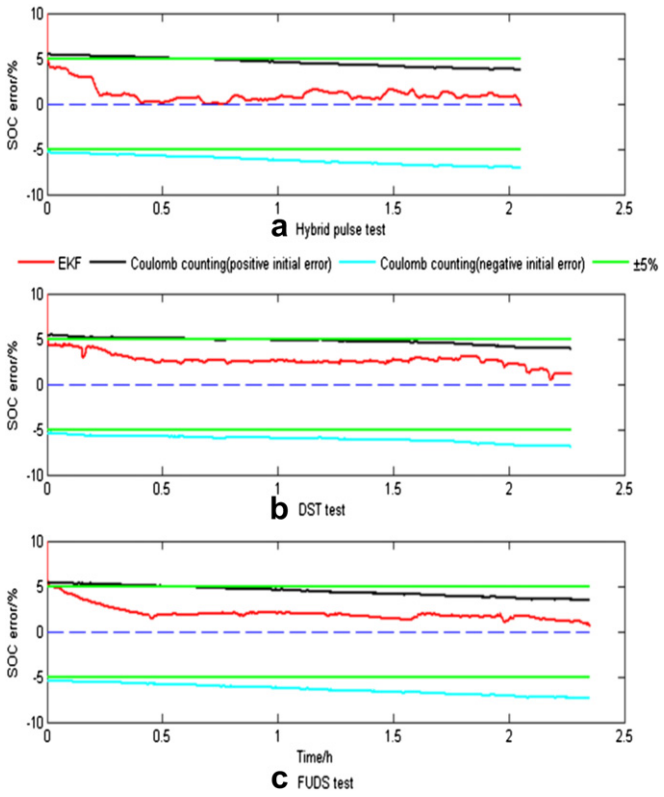

Fig. 13. SOC estimation errors of the $LiFePO_4$ cell under 22 °C (before aging), (a) hybrid pulse test; (b) DST test; (c) FUDS test.

evaluate the SOC estimator, its performance is compared against the Coulomb counting method.

(1) LiNMC cell

The OCV is often used to determine the initial SOC of Coulomb counting using the OCV–SOC relationship. The OCV error thus leads to the initialization error for Coulomb counting. Based on the fact that the practically available cell-level precision is around 0.1% [31], the OCV error incurred by voltage sensor is thus around 4 mV. Furthermore, in practice OCV measurement is subject to electromagnetic interference, switching of high-current loads in nearby wiring and insufficient relaxation. Sometimes insufficient relaxation can induce a voltage measurement error of 20 mV [32]. Based on these considerations, we assume that the absolute measurement error of the cell OCV is 8 mV. The maximum initial SOC error of the Coulomb counting method can be algebraically calculated based on this assumed OCV error and the SOC–OCV curve. The results are summarized in Table 8.

The initial error of the EKF is assumed to be 10%. The initial values of the EKF prediction and correction gain matrices are fixed for all cases. Note that both the EKF and Coulomb counting use the corrupted current measurement in their SOC estimation. Fig. 11 shows the SOC estimation results for 22 °C. It can be seen that the EKF-based estimator efficiently compensates for the initial error and has a better accuracy than Coulomb counting for both the training and validation datasets. The biased current noise has a larger negative impact to the Coulomb counting method than to the EKF. The results under 10 °C and 35 °C are similar. To more clearly compare the overall performance of the EKF and Coulomb counting, the RMS SOC estimation errors under three temperatures are shown in Fig. 12. It is obvious that the EKF SOC estimator has better accuracy. Since the model has an inferior accuracy in the validation data (DST/FUDS dataset excluding the data below 20% SOC) to that in the training data (hybrid pulse test dataset excluding

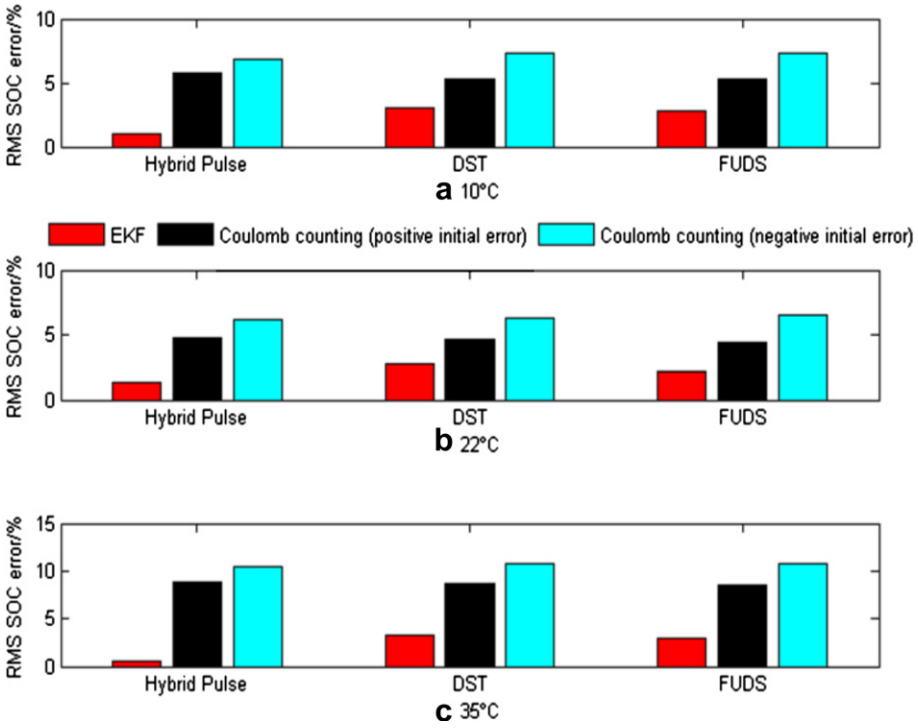

Fig. 14. RMS SOC errors under three temperatures for the $LiFePO_4$ cell (new cell).

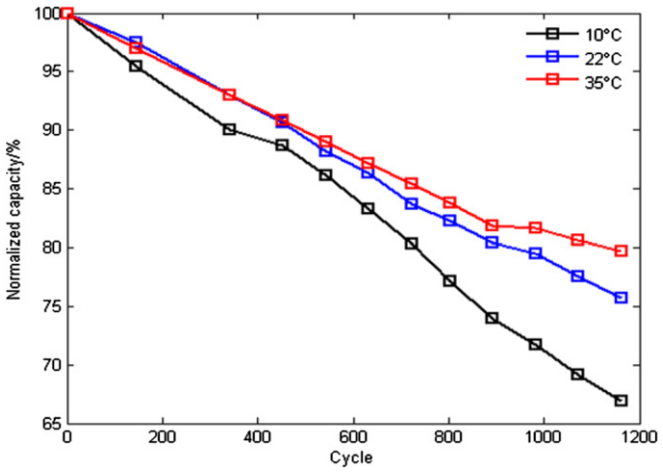

Fig. 15. Normalized capacities of the LiNMC cell in the aging process.

the data below 20% SOC), the error of SOC estimation in the validation data is always higher. The estimation errors in the validation datasets under three temperatures are around 1%, indicating a good robustness against varying loading profiles and temperatures.

(2) $LiFePO_4$ cell

The initial SOC error of Coulomb counting for the $LiFePO_4$ cell is determined using the same method as the LiNMC cell. Again assuming a voltage measurement error of 8 mV, the results for the $LiFePO_4$ cell are shown in Table 9. The errors are larger than those of the LiNMC cell, due to the flatter OCV–SOC curves. The SOC estimation errors under 22 °C are shown in Fig. 13. The RMS SOC errors under three temperatures are shown in Fig. 14. The results are similar to those of the LiNMC cells. Further, we can see that there is an obvious difference in estimation errors between the training and validation datasets. Due to the flatter OCV, the SOC estimation of the $LiFePO_4$ cell is more susceptible to model error. The validation errors are around 2.5%, higher than the 1% accuracy achieved on the LiNMC cells.

4.2. Robustness against cell aging

The battery cells always degrade with time in real operations. The degradation is manifested as capacity or power losses. The capacity loss is partially due to loss of cyclable Li Ions caused by multiple factors, such as cathode structure degradation, side reactions, passivation form and lithium plating at the anode [33]. The power loss is mainly due to the increase in cell resistance. It is important to study the robustness of the SOC estimator since robustness against cell aging is of great significance for BMS of electrified vehicles.

(1) LiNMC cell

Fig. 15 shows the calibrated capacities under three temperatures in the degradation process of the LiNMC cell at 22 °C. Here, we used data up to cell age of 342 cycles at 22 °C to analyze the robustness of the EKF estimator. The capacity reduced by about 10% at 10 °C when the cell is 342 cycles old at 22 °C—which is roughly half way through the typical life expectancy accepted for automotive applications (a battery pack is determined to be "at the end of its life" when its capacity loss reaches 20%). The three characterization test

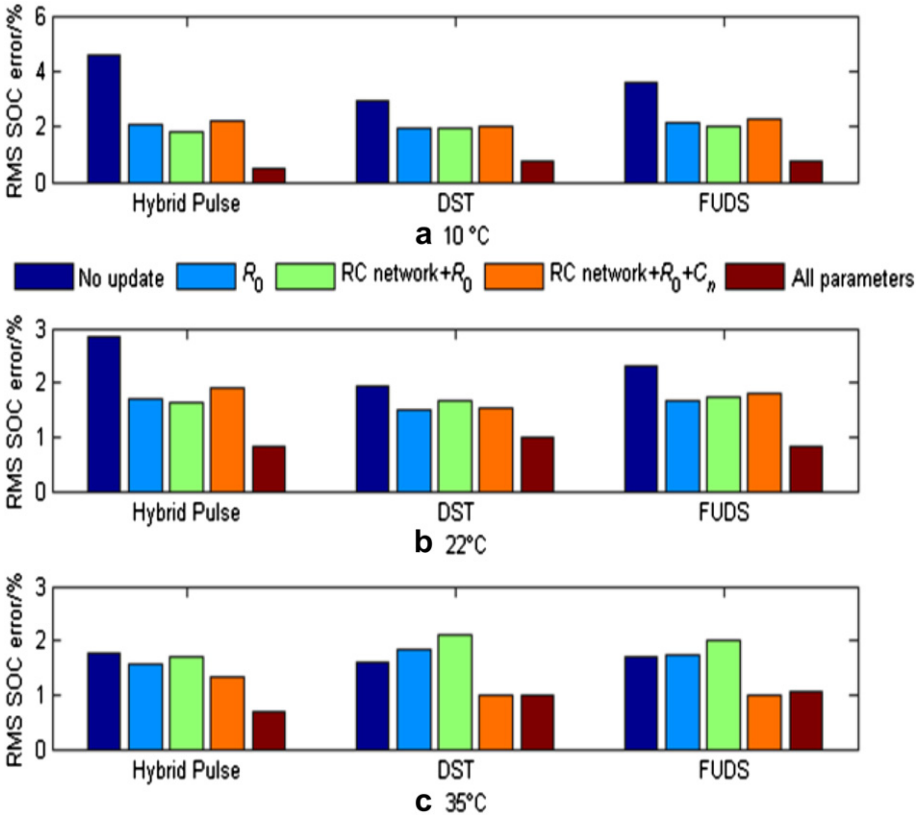

Fig. 16. Comparison results of a sequence of estimators for the LiNMC cell (after aging) with different level of model parameter update.

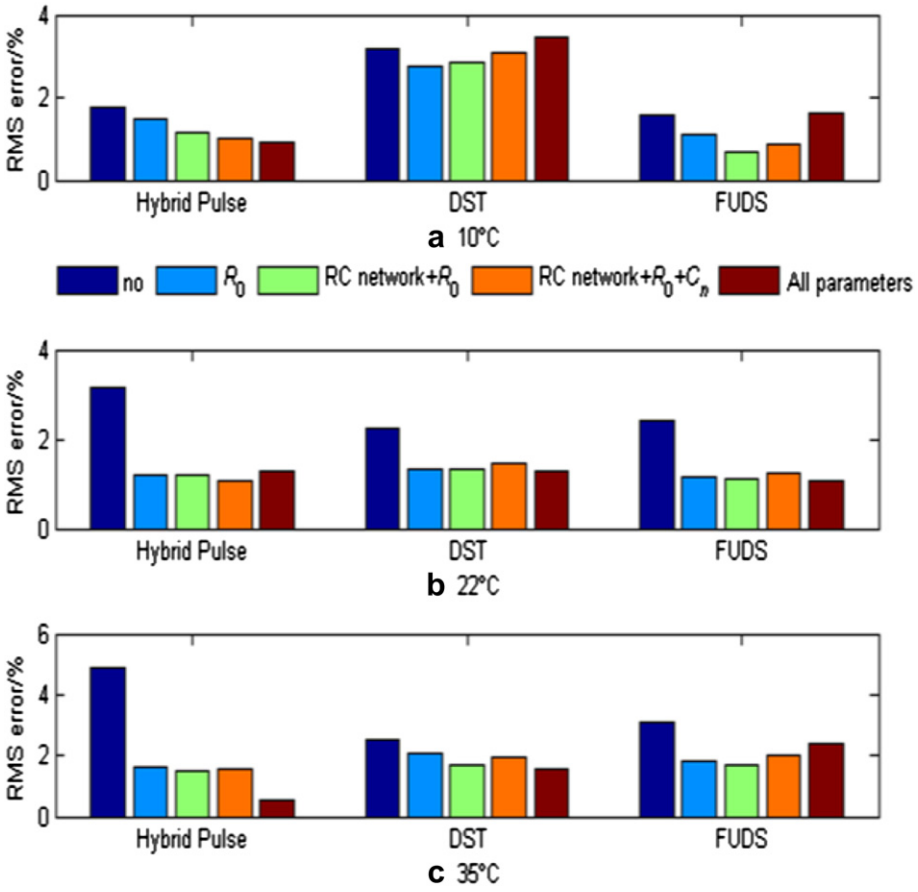

Fig. 17. Comparison results of a sequence of estimators for the $LiFePO_4$ cell (after aging) with different level of model parameter update.

datasets right after 342 cycles are used to evaluate the SOC estimator. The initial SOC error and tuning parameters of the EKF are kept unchanged when we compare a sequence of estimators with increasing level of parameter updates. Fig. 16 shows the comparison results. It can be seen that if no parameters, including the capacity C_n, are updated, the estimator performance deteriorates significantly. The RMS errors of the SOC estimation are clearly larger than those shown in Fig. 12. Updating internal ohmic resistance R_0 can improve the SOC estimation in most cases. Updating parameters of the RC network in addition to R_0 does not help much. If we update all model parameters, including the cell capacity C_n, the RMS error can be reduced to below 1% in most cases.

It should be noted that updating some of the model parameters is quite easy to do. For example, the internal ohmic resistance R_0 can be easily obtained even under simple pulse loads. This simple update reduces model prediction error by more than half. Updating RC parameters or the cell capacity is harder onboard. It may be possible to obtain those model parameters during charging process, when the charging current can be manipulated and more computation power is available.

(2) $LiFePO_4$ cell

The $LiFePO_4$ cells we tested show much slower degradation. We have finished 2600 cycles and the capacity loss at 22 °C is only around 3%. The three characterization test datasets collected right after 2587 cycles are used. The RMS errors of the estimators with different levels of model parameter updates are shown in Fig. 17. Again, the estimator without parameter update shows poor performance—this is because while the cell capacity does not reduce significantly, its dynamic behavior changes noticeably. The RMS errors in the training datasets (hybrid pulse test) are worse than the LiNMC cell, due to the very flat OCV–SOC curve of the $LiFePO_4$ cell. The RMS errors in the validation datasets (DST and FUDS) are similar to the LiNMC cell. The nominal model of the $LiFePO_4$ cell is less accurate after degradation. Also, updating internal resistance R_0 improves the robustness of the SOC estimator noticeably. Updating the RC network and capacity does not help much, since capacity loss is small. If all the model parameters are updated, the SOC estimator has the best robustness based on the overall evaluation of all the 9 datasets. In practice, however, it is challenging to update all the model parameters. Considering both the model accuracy and requirement for parameter update, we concluded that updating the internal resistance is the most cost-effective update one can use to improve the robustness of SOC estimation method against cell aging.

5. Conclusions

The robustness of SOC estimation algorithms of two types of Li-ion batteries is studied against varying loading profiles, temperatures and aging levels. The preferred model structures determined in our previous work [24] for the LiNMC and $LiFePO_4$ cells are used. The optimal functions of SOC and temperature explicitly describing the model parameters are selected from commonly used generic functions for battery modeling. The sixth-degree polynomial is found to depict OCVs of both cells well. The exponential function is determined to be the best for the RC parameters of the first-order RC model for the LiNMC cell; the third-degree polynomial is preferred for the RC and hysteresis parameters of the first-order RC

model with hysteresis for the $LiFePO_4$ cell. The coefficients of these generic functions are optimized by a combined MPSO and SQP procedure. Based on the optimal model parameters, the Extended Kalman Filter technique is used to estimate the battery SOC. Given the training datasets from new cells, the robustness of the SOC estimator against varying loading profiles and temperatures is evaluated and compared against the Coulomb counting method. The EKF-based estimator performs better than the Coulomb counting method, and the RMS estimation errors under validation datasets under three temperatures are around 1% and 2.5% for the LiNMC and $LiFePO_4$ cells, respectively. Due to a flatter OCV–SOC surface, the SOC estimation of the $LiFePO_4$ cell is more vulnerable to cell aging and if the model is not updated, its performance was found to be unacceptable. Updating the internal ohmic resistance of the nominal model improves the performance of the estimator significantly (by about half). Updating all the model parameters achieves even better performance however this may not be easy to achieve in real-time driving.

Acknowledgment

This work was supported by the Automotive Research Center (ARC), a U.S. Army center of excellence in modeling and simulation of ground vehicles.

References

[1] J.H. Aylor, A. Thieme, B.W. Johnson, IEEE Trans. Ind. Electron 39 (1992) 398–409.
[2] T. Liu, D. Chen, C. Fang, Int. J. Electron 87 (2000) 211–226.
[3] Y. Çadırcı, Y. Özkazanç, J. Power Sources 129 (2004) 330–342.
[4] Y. Hu, Identification and state estimation for linear parameter varying systems with application to battery management system design, Ph.D. dissertation, Ohio State University (2010).
[5] C.C. Chan, E.W.C. Lo, W. Shen, J. Power Sources 87 (2000) 201–204.
[6] W. Shen, K.T. Chau, C.C. Chan, IEEE Trans. Veh. Technol. 54 (2005) 1705–1712.
[7] B. Cheng, Z. Bai, B. Cao, Energy Convers. Manage. 49 (2008) 2788–2794.
[8] A.J. Salkind, C. Fennie, P. Singh, T. Atwater, D.E. Reisne, J. Power Sources 80 (1999) 293–300.
[9] P. Singh, R. Vinjamu, X. Wang, D. Reisne, J. Power Sources 162 (2006) 829–836.
[10] T. Hansen, C. Wang, J. Power Sources 141 (2005) 351–358.
[11] Q. Shi, C. Zhang, N. Cui, Int. J. Automot. Technol. 9 (2008) 759–764.
[12] G.L. Plett, J. Power Sources 134 (2004) 252–261.
[13] G.L. Plett, J. Power Sources 134 (2004) 262–276.
[14] G.L. Plett, J. Power Sources 134 (2004) 277–292.
[15] G.L. Plett, J. Power Sources 161 (2006) 1356–1368.
[16] G.L. Plett, J. Power Sources 161 (2006) 1369–1384.
[17] S. Santhanagopalan, R.E. White, Int. J. Energy Res. 34 (2010) 152–163.
[18] J.Y. Han, D.C. Kim, M. Sunwoo, J. Power Sources 188 (2009) 606–612.
[19] J. Wang, J. Guo, L. Ding, Energy Convers. Manage. 50 (2009) 3182–3186.
[20] F. Sun, X. Hu, Y. Zou, S. Li, Energy 36 (2011) 3531–3540.
[21] I.S. Kim, J. Power Sources 163 (2006) 584–590.
[22] I.S. Kim, IEEE Trans. Power Electron 23 (2008) 2027–2034.
[23] Y. Hu, S. Yurkovich, J. Power Sources 198 (2012) 338–350.
[24] X. Hu, S. Li, H. Peng, J. Power Sources 198 (2012) 359–367.
[25] Y. Hu, S. Yurkovich, Y. Guezennec, B.J. Yurkovich, Control Eng. Pract. 17 (2009) 1190–1201.
[26] Y. Hu, S. Yurkovich, Y. Guezennec, B.J. Yurkovich, J. Power Sources 196 (2011) 449–457.
[27] D.E. Neumann, S. Lichte, A Multi-Dimensional Battery Discharge Model with Thermal Feedback Applied to a Lithium-ion Battery Pack, NDIA Ground Vehicle Systems Engineering and Technology Symposium-Modeling & Simulation, Testing and Validation (MSTV) Mini-Symposium, 2011.
[28] M. Chen, G.A. Rincón-Mora, IEEE Trans. Energy Convers. 21 (2006) 504–511.
[29] A. Szumanowski, Y. Chang, IEEE Trans. Veh. Technol. 57 (2008) 1425–1432.
[30] MATLAB, Curve Fitting Toolbox™ 2, User's Guide, The MathWorks Inc., 2010.
[31] http://www.maxim-ic.com/MAX17830.
[32] J. Qian, Rechargeable Battery Characteristics, Safety, Charging and Fuel Gauges, Technical Presentation, Texas Instruments Inc., 2009.http://focus.ti.com/asia/download/TechDay09cn_Analog_Power_1_Battery_chemistry_fuel_gauge.pdf.
[33] M. Alamgir, A.M. Sastry, Efficient batteries for transportation applications, SAE paper (08CNVG-0036), 2008.